A Self-Sensing Approach for Dielectric Elastomer Actuators Based on Online Estimation Algorithms

A Self-Sensing Approach for Dielectric Elastomer Actuators Based on Online Estimation Algorithms

Gianluca Rizzello, David Naso, *Senior Member, IEEE,* Alexander York, Stefan Seelecke

***Abstract*— This paper investigates the capability of self-sensing in a position actuator based on a dielectric elastomer membrane. The approach uses voltage and current measurements to estimate electrical resistance and capacitance online, by injecting a high-frequency low-amplitude voltage component in the actuation signal. The actual deformation is subsequently reconstructed using a model-based estimate of the electrical parameters, implemented on a FPGA platform with a sampling frequency of 20 kHz. The main peculiarity of the approach is the use of recursive identification and filtering algorithms that avoid the need of charge measurements. The self-sensing algorithm is extensively validated on a precision linear-motion actuator, which uses a non-linear biasing system to obtain large actuation strokes.**

***Index Terms*—Dielectric Elastomer, Dielectric Electro-Active Polymer, Self-Sensing, Smart Materials.**

I. Introduction

Dielectric Elastomers (DE), also known as Dielectric Electro-Active Polymers, represent a family of smart materials in which the application of an electric field between compliant electrodes placed on the elastomer surface generates a controllable deformation. Such actuation principle can be exploited to generate different kind of actuation modes [1], [2]. Prototypes of DE Actuators (DEA) operating as pumps [3], valves [4], robots [5], and micropositioning stages [6] have been documented in recent literature. In comparison with other smart materials, DE offer relatively large deformation, high energy density, low power consumption and fast dynamic response. As for most actuators based on smart materials actuators, another attractive characteristic of DEA is the possibility to perform self-sensing of output variables or, in other words, to use the polymer simultaneously as sensor and actuator [7], [8]. In fact, the electrical response of the material is influenced by the instantaneous state of deformation, since the material electrical parameters (i.e. capacitance, resistance, and inductance) change with the geometry of the material. By performing electrical measurements while actuating, one can reconstruct the material deformation and use it in various ways, for example, as a feedback signal for a position control algorithm [9], [10]. This is particularly significant in micrometric positioning systems because it eliminates the need of an additional precise position sensor which, in many applications, is the most expensive component of the system [11]. Moreover, self-sensing can be performed without any additional sensing hardware as electrical measurements such as voltage and current are typically available from the same electronic circuit used to drive the actuator.

To enable self-sensing, the relationship between the electrical behavior of the material and its state of deformation needs to be characterized and modeled [12]–[16]. Several authors have proposed sensor applications based on DE membranes [17]–[20], and a number of authors also considered the possibility of combining sensing with actuation. For instance, in [21] self-sensing is performed by constructing a RC high-pass filter whose capacitive element is represented by the DEA. By applying a sinusoidal excitation and measuring the voltage on the series resistor by means of an oscilloscope, the electrical impedance is acquired and then used to reconstruct the applied force. The paper includes some preliminary results without an explicit validation of the estimated force. A similar experimental hardware is used in [22], in which the approach is validated at several actuation frequencies. The authors represent the DEA as a pure capacitor, thus neglecting the resistance of the electrodes. Since the approximation of the DEA dynamics as a pure capacitor does not hold at high frequencies, it may generate significant sensing errors as the sensing frequency increases. Moreover, the approach requires a peak detection method to reconstruct the sensed variable, which complicates the overall implementation. Matysek *et al.* present in [23] an electronic circuit capable to drive and sense up to 8 DEA devices for a tactile display. The approach uses the integration of the measured current in some predefined time interval to estimate the charge and then the capacitance. In [24] a regression algorithm based on measurement of charge, voltage and current is proposed to obtain capacitance measurements taking into account resistive effects. As clarified in [25], this approach requires pulse width modulation in the voltage

The authors would like to acknowledge support of Parker Hannifin, BioCare Business Unit.

G. Rizzello and D. Naso are with the Department of Electrical and Information Engineering, Politecnico di Bari, Bari, IT (e-mail: gianluca.rizzello@poliba.it, david.naso@poliba.it).

A. York and S. Seelecke are with the Department of Mechatronics, Universität des Saarlandes, Saarbrücken, DE (e-mail: alexander.york@mmsl.uni-saarland.de, stefan.seelecke@mmsl.uni-saarland.de).

amplification, therefore it is designed for a specific hardware. The same algorithm is also used in [26] to perform closed loop control of various types of materials. In [27], Hoffstadt et al. present and experimentally test a frequency domain self-sensing algorithm, which exploits the high-frequency oscillations of a dual active bridge to estimate both the DEA capacitance and series resistance from voltage and current measurements. Also in this case, the implementation of the proposed method requires specific hardware and peak/phase detection algorithms.

Following the research trends emerging in the aforementioned references, this paper proposes a new self-sensing method for DEAs. The approach is based on a recursive parameter identification method that has relatively low implementation effort, is suitable for real-time applications and has a good accuracy. In particular, the approach does not use peak detection algorithms, and requires only voltage and current measurements. Additional digital filters, i.e. low-pass and comb filters, are included to obtain further noise rejection and improvement in accuracy. The method is validated with an extensive experimental investigation, in a wide set of experimental conditions and up to an actuation frequency of 10 Hz. A circular membrane with a bistable biasing system is considered as a case study for the experimental validation of the proposed methodology. In particular, the bistable biasing element introduces further nonlinearities to the system, making it a challenging platform to test the self-sensing approach in realistic operative condition. The present paper is an extension of the preliminary ideas presented in the paper [28].

The reminder of this paper is organized as follows. Section II presents the DEA operating principle and modeling, while Section III illustrates the self-sensing algorithm. Experimental results are shown in Section IV, and section V draws some conclusions and ideas for future developments.

II. DEA Electrical Model

A DEA consists of a polymeric film material (i.e. silicone, acrylic elastomer) with compliant electrodes printed over the external surfaces, forming a compliant capacitor. When a voltage is applied to the electrodes, the resulting electric field in the polymeric film generates compressive forces that induce a reduction in thickness and a subsequent expansion in area. The mechanical compressive stress which arises in the thickness axis of the membrane as a consequence of the electric field is typically referred as Maxwell stress, and is given by the following equation

$$\sigma_M = -\varepsilon_0 \varepsilon_r E^2 , \quad (1)$$

where the void permittivity ε_0 and the polymer relative permittivity ε_r act as proportional factors between the square of the electric field E and the Maxwell stress σ_M. Thus (1) describes the electromechanical transduction principle of DEAs.

A. Actuator Description

This work focuses on the DEA shown in Fig. 1 (a), consisting of a circular membrane which operates out-of-plane. The outer and inner frames (green) are made of rigid plastic, while the intermediate ring is constituted by a 50 μm DEA silicon film (gray) surrounded by carbon based electrodes (black). A mechanical pre-stretch is also applied during the membrane manufacturing process, resulting into an actual thickness of 40 μm. In order to prevent electrical breakdown, the maximum voltage is set to a safety value of 2.5 kV.

In order to generate motion, a biasing force provided by means of mechanical elements, such as masses or springs, must be applied to the membrane. As remarked in [29], the choice of the biasing elements strongly affects the actuation performance. The biasing mechanism considered in this paper consists of a combination of a Negative-Rate Biasing Spring (NBS), i.e. a bi-stable nonlinear spring, and a Linear Biasing Spring (LBS). The adoption of the NBS produces a dramatic increase in stroke with respect to other biasing solutions, i.e., linear springs or masses [29], but it increases the number of nonlinear phenomena that must be taken into account. In particular, when the NBS is used as biasing element, a large voltage-displacement hysteresis is observed. It has to be remarked that such hysteresis does not represent a limitation from the application point of view, as it can be effectively compensated by means of feedback control laws of relatively low complexity [30]. Fig. 1 shows a sketch of the NBS-LBS-DEA system in the unactuated (b) and actuated (c) configuration.

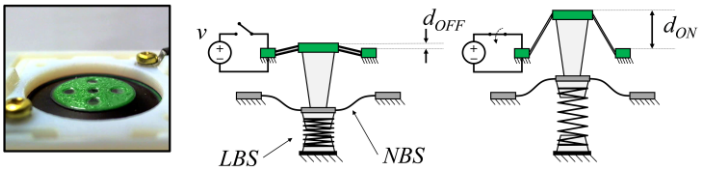

Fig. 1. DEA circular membrane (a), DEA biased with LBS + NBS, voltage OFF (b) and ON (c).

B. Electrical Model

A DEA is essentially a compliant capacitor, but a description based on a RC circuit rather than a simple capacitive element, see e.g. [15], [23], [31], is more frequently used in order to take into account the electrical dissipation. The parameters of the equivalent circuit of the DEA strongly depend on the geometry, which changes during the actuation, making it necessary to use nonlinear or time-varying models of the phenomenon. The typical circuit used for modeling a DEA is shown in Fig. 2. C is the DEA capacitance, R_l models the leakage resistance of the material, R_e represents the resistance of the electrodes, and R_a is an external resistor, which, in general, represents connection cables or a filtering resistor. Each electrical element related to the DEA depends on the current state of deformation of the membrane, which is described in terms of out-of-plane stroke d. The electrical

quantities of interest are the applied voltage v, the resulting current i, and the electric charge on the capacitor q. After defining the overall series resistance as

$$R_s(d) = R_a + 2R_e(d), \tag{2}$$

the circuit in Fig. 2 can be described by means of the following state-space model

$$\begin{cases} \dfrac{d}{dt}q = -\left[\dfrac{1}{R_l(d)C(d)} + \dfrac{1}{R_s(d)C(d)}\right]q + \dfrac{1}{R_s(d)}v \\ i = -\dfrac{1}{R_s(d)C(d)}q + \dfrac{1}{R_s(d)}v \end{cases}. \tag{3}$$

All the coefficients in equation (3) are expressed as functions of the out-of-plane deformation d. As reported in [15], this model provides sufficient accuracy in describing several practical operating conditions of the device.

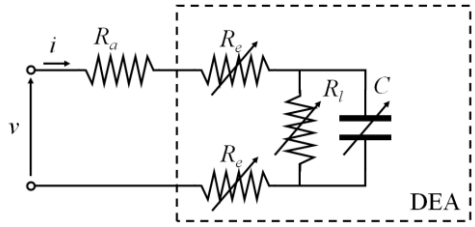

Fig. 2. DEA equivalent circuit.

III. Self-Sensing Algorithm

As discussed above, the coefficients affecting the DEA electrical response are strongly dependent on the deformation. In principle, model (3) can be inverted and used to predict the state of deformation, using voltage and current as inputs. However, such an inversion, even if analytically tractable, is not particularly useful. In fact, typical values of the leakage resistance (order of GΩ) are orders of magnitude larger than the series resistance (order of MΩ), leading to a very small steady-state current. When this is the case, small uncertainties in the model parameters and measurement bias tend to produce a significant drift in the estimated charge, making the displacement reconstruction by means of the model ineffective.

The idea proposed in this paper is instead to use the structure of the model equations in conjunction with an online identification algorithm. This solution enables real-time estimation of the model coefficients that minimize the difference between the measured and predicted signals. The approach requires voltage and current measurement only, without any prior information on model coefficients. Moreover, several recursive identification algorithms are available for solving the real-time estimation problem [32]. As remarked in Section II, the series resistance shows a nonlinear, hysteretic dependence on the deformation, and therefore it is not suitable for self-sensing. The leakage resistance, instead, may be too large in comparison with the series resistance, and therefore hard to be accurately estimated if the adopted current sensor has a limited accuracy. On the other hand, the capacitance-deformation relationship is monotonic and non-hysteretic, so it can be effectively employed for self-sensing. Fig. 3 shows an example of an experimental capacitance-displacement curve recorded with a Hameg® LCR-bridge model HM8118. The curve shows a parabolic trend, in agreement with the physical model developed in [15]. On the other hand, measurements of DEA resistances are omitted in this paper, as the LCR-bridge showed some difficulties when trying to record their values.

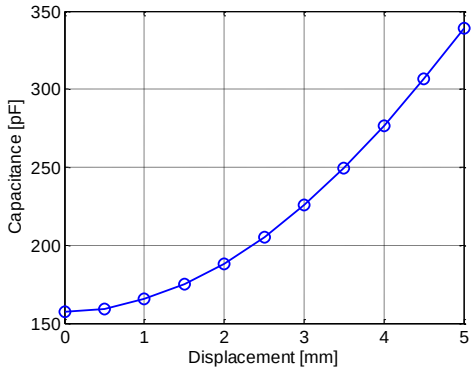

Fig. 3. DEA measured capacitance for different deformations.

As (3) is a high-pass filter, the current resulting from a low-frequency actuation, with typical values of leakage resistance, is not large enough to be accurately measured. For this reason, when performing self-sensing, the DEA must be driven by a composite signal consisting of the sum of two contributions with different harmonic content [22]. An example of such signal is shown in Fig. 4, where the low and high frequency are chosen equal to 1 and 50 Hz sinewaves, respectively. The high-amplitude, low-frequency component is responsible for the electromechanical actuation but the resulting current is negligible. Conversely, the low-amplitude, high-frequency component does not produce motion as it is filtered by the actuator mechanical bandwidth, while it generates a current signal which is large enough to be accurately measured.

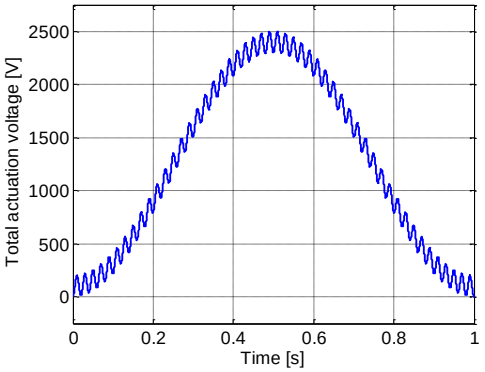

Fig. 4. Actuation signal for self-sensing, consisting of the sum of a 1 Hz and a 50 Hz harmonic components.

A. *Online parameter estimation based on full model*

When a composite voltage signal as the one in Fig. 4 is applied to the DEA, it is expected that the current response will exhibit the same high-frequency dynamics of the input, while the capacitive and resistive coefficients will vary in a much slower way according to the mechanical deformation

induced by the low-frequency voltage component. Under the additional requirement of sufficiently fast sampling, it is realistic to assume that the changes in capacitance and resistances between two successive samples will be significantly smaller than the changes in voltage and current, and therefore that they can be approximated as constant terms, i.e.

$$C_{k+1} \approx C_k,\ R_{s,k+1} \approx R_{s,k},\ R_{l,k+1} \approx R_{l,k}, \tag{4}$$

where the subscript k denotes the discretized time. If the derivative is approximated with the forward Euler method,

$$\frac{d}{dt}q \approx \frac{q_{k+1}-q_k}{T_s}, \tag{5}$$

where T_s is the sampling time, system (3) can be approximated in the discrete time as follows:

$$\begin{cases} \dfrac{q_{k+1}-q_k}{T_s} = -\left(\dfrac{1}{R_{l,k}C_k}+\dfrac{1}{R_{s,k}C_k}\right)q_k + \dfrac{1}{R_{s,k}}v_k \\ i_k = -\dfrac{1}{R_{s,k}C_k}q_k + \dfrac{1}{R_{s,k}}v_k \end{cases}. \tag{6}$$

The state-space model (6) can then be reformulated as the following difference equation

$$v_k = \left(1-\frac{T_s}{R_{l,k}C_k}\right)v_{k-1} + R_{s,k}i_k + \left(\frac{T_s}{C_k}+\frac{R_{s,k}T_s}{R_{l,k}C_k}-R_{s,k}\right)i_{k-1}. \tag{7}$$

Finally, equation (7) can be written in the following Linear In Parameters (LIP) form as follows

$$y_k = \varphi_k{}^T\theta_k, \tag{8}$$

with

$$y_k = v_k, \tag{9}$$

$$\varphi_k = \begin{bmatrix} v_{k-1} & i_k & i_{k-1} \end{bmatrix}^T, \tag{10}$$

$$\theta_k = \left[\left(1-\frac{T_s}{R_{l,k}C_k}\right) \quad R_{s,k} \quad \left(\frac{T_s}{C_k}+\frac{R_{s,k}T_s}{R_{l,k}C_k}-R_{s,k}\right)\right]^T. \tag{11}$$

Assuming that y_k and φ_k can be measured online (which is the case), the LIP structure of equation (7) allows to perform real-time estimation of the unknown coefficients vector θ_k by means of online regression algorithms. In this work, we focus on the standard RLS [32]. Alternative choices are possible, e.g. Least Mean Squares (LMS), see [32] for further details), even if in [28] it is shown that RLS provides faster and more accurate estimations than LMS (at the expense of a higher computational effort). We also remark that performance comparison between RLS and LMS represents a topic which has been investigated by several authors, see e.g. [33]–[35]. The RLS updates the estimation according to the following algorithm

$$\begin{cases} \hat{\theta}_k = \hat{\theta}_{k-1} + \dfrac{P_{k-1}\varphi_k}{1+\varphi^T{}_k P_{k-1}\varphi_k}\left(y_k - \varphi^T{}_k\hat{\theta}_{k-1}\right) \\ P_k = \dfrac{1}{\mu}\left(P_{k-1} - \dfrac{P_{k-1}\varphi_k\varphi^T{}_k P_{k-1}}{1+\varphi^T{}_k P_{k-1}\varphi_k}\right) \end{cases}. \tag{12}$$

where notation $\hat{\theta}_k$ represents the estimate of θ at the *k-th* sampling time. The coefficient $\mu \leq 1$ is the forgetting factor, a tuning parameter that permits to take into account the time-varying behavior of θ_k. The smaller μ, the faster is the RLS in tracking time-varying parameters, but the effects of the noise are consequently amplified. Coefficient μ needs to be properly tuned by taking into account the trade-off between estimation speed and noise filtering. A simple empirical rule for setting μ is the following one:

$$\mu = 1-\frac{1}{W}. \tag{13}$$

This rule gives more emphasis on the last W samples of the prediction error. It is worth mentioning that standard implementation of RLS algorithm provided by (12) may be affected by numerical instability due to propagation of round-off error [36]. In such case, different implementations of the algorithm need to be considered. However, as (12) did not show such numerical instability in our experiments, we did not considered alternative implementation in this work.

Once the estimate $\hat{\theta}_k$ is obtained, the corresponding capacitance and resistances estimations are given by

$$\begin{bmatrix} \hat{C}_k & \hat{R}_{s,k} & \hat{R}_{l,k} \end{bmatrix} = \left[\frac{T_s}{\hat{\theta}_{1,k}\hat{\theta}_{2,k}+\hat{\theta}_{3,k}} \quad \hat{\theta}_{2,k} \quad \frac{\hat{\theta}_{1,k}\hat{\theta}_{2,k}+\hat{\theta}_{3,k}}{1-\hat{\theta}_{1,k}}\right], \tag{14}$$

with

$$\hat{\theta}_k = \begin{bmatrix} \hat{\theta}_{1,k} & \hat{\theta}_{2,k} & \hat{\theta}_{3,k} \end{bmatrix}. \tag{15}$$

B. Online parameter estimation based on simplified model

In principle, the approach presented in the previous section could be used to perform online estimation of all DEA parameters, but it is obviously preferable to restrict the online identification to the smallest subset of parameters with a significant influence on the variable of interest. Moreover, the sensitivity of the response on the model parameters is strongly related to the frequency used for self-sensing, hereafter indicated as f_e. In fact, it is possible to prove that the voltage-current transfer function corresponding to (3) is characterized by a stable pole and a stable zero, whose cut-off frequencies f_p and f_z can be calculated as follows [28]

$$f_p = \frac{1}{2\pi C}\left(\frac{1}{R_l}+\frac{1}{R_s}\right) \approx \frac{1}{2\pi C R_s} \quad (if\ R_l\ ?\ R_s) \tag{16}$$

$$f_z = \frac{1}{2\pi C R_l} \tag{17}$$

If the frequency f_e is sufficiently far away from f_p or f_z, we can neglect the effects of the corresponding zero or pole from the transfer function without introducing a significant error. Note that f_z depends on R_l, while f_p is mainly related to R_s. Such considerations are only valid for constant or slow-varying deformations.

The first proposed approximation regards to the leakage resistance. If the sensing frequency f_e is such that

$$f_z = f_e, \tag{18}$$

then we can assume that the effects of the zero generated by the leakage resistance are negligible. Typical values of leakage resistance (order of MΩ) and capacitance (order of fractions of nF) lead to f_z of the order of fractions of Hz. Therefore,

condition (18) is often true for typical values of f_e of hundreds or thousands of Hz. Condition (18) is particularly true when the leakage resistance is very large (i.e., the leakage current is very small). In fact, if (18) is true, it can be assumed that

$$f_z = \frac{1}{2\pi R_l C} \approx 0 \rightarrow R_l = \infty \,, \tag{19}$$

which implies that model (6) is equivalent to the following difference equation

$$v_k - v_{k-1} = R_{s,k} i_k + \left(\frac{T_s}{C_k} - R_{s,k} \right) i_{k-1} \,. \tag{20}$$

Equation (20) corresponds to the RC series model portrayed in Fig. 5 (b) and is valid for high-frequency regimes. The new model (20) corresponds to a new regression problem, which can be addressed with the same online estimation technique discussed in Section III.A.

The second simplification considers the case in which f_e is much larger than the zero cut-off frequency and, at the same time, much smaller than the pole cut-off frequency, namely (18) must hold in combination with

$$f_e = f_p \,. \tag{21}$$

If (18) and (21) hold true, we can neglect the effects of both leakage and electrodes resistance, and therefore assume that the DEA behaves as a pure capacitor. Even if this is a strong approximation, as mentioned in the previous section it is commonly adopted in DEA sensing applications, e.g. [18], [22]. Typical values of electrodes resistance (order of fractions of MΩ) results into a f_p of the order of kHz. This frequency is close to typical values of f_e, therefore the purely capacitive approximation must be performed carefully. Reducing f_e in order to meet (21) does not overcome the problem, because if f_e is not large enough, it may happen that the resulting current is too low to be measured or f_e may not be large enough in comparison to the mechanical frequency, thus violating (4), and possibly introducing additional mechanical vibrations. Thus, the selection of the sensing frequency and the consequent model for self-sensing must be performed depending on the individual application. If (21) is admissible, we have

$$f_z \approx \frac{1}{2\pi R_s C} \approx \infty \rightarrow R_s = 0 \,, \tag{22}$$

therefore the approximation holds for small values of electrodes resistance. Combining (19) and (22), the model (6) is approximately equivalent to the following regression problem, which can be again addressed via RLS

$$v_k - v_{k-1} = \frac{T_s}{C_k} i_{k-1} \,. \tag{23}$$

Finally, we point out the case in which only the leakage resistance is considered, while neglecting the electrodes resistance is not considered here. Even if theoretically tractable, this case is not of practical interest for self-sensing because, for typical values of DEA electrical parameters, the model including only the leakage resistance is valid for very low frequencies (some Hz), while self-sensing applications are typically focused on high frequency (hundreds or thousands of Hz). Nevertheless, the development of the equations for this particular case can be obtained in a straightforward way, and therefore omitted.

A further useful remark regards the fact that the outputs of both regressions in (20) and (23) contain the derivative of the measured voltage. This differentiation may introduce additional noise, which can be partially compensated by using the filtering technique discussed in the next section.

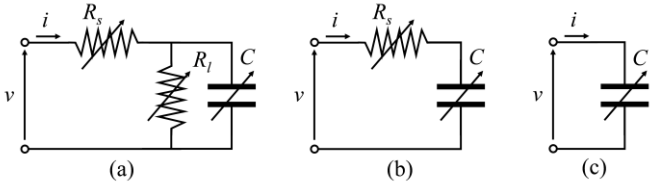

Fig. 5. Different DEA electrical models, complete model (a), capacitance plus series resistance approximation (b) and pure capacitance approximation (c).

C. Filtering

The degradation of the performance of the estimation process caused by the measurement noise can be attenuated by using appropriate pre- and post-filtering. In order to reduce the noise amplification due to the differentiation, or to reduce the measurement noise in general, it is possible to apply a low-pass filter to both members of (8) (e.g. a first order low-pass filter). The filter bandwidth must be wide enough to preserve significant components of the signals. The new filtered version of equation (8), assuming small variations on θ_k, is given by

$$y'_k = \varphi'^{\,T}_k \, \theta_k \,, \tag{24}$$

with

$$y'_k = F(z) y_k \,, \tag{25}$$

$$\varphi'_k = F(z) \varphi_k \,, \tag{26}$$

and $F(z)$ is the chosen filter transfer function. In case of vector-values quantities, the scalar filter is applied on each component of y_k and φ_k.

It has been experimentally observed that capacitance and resistance estimations are affected by high-frequency noise and disturbances at frequencies that are multiples of the sensing signal frequency. For this reason, it may be useful to perform additional post-filtering to remove these undesired harmonic components [37]. We first define the quantity M, representing the ratio between sampling frequency f_s, reciprocal of the sampling time T_s, and sensing signal frequency f_e

$$M = \frac{f_s}{f_e} \,. \tag{27}$$

The filter can be chosen as a notch filter

$$H(z) = b_0 \frac{1 - 2\cos\left(\frac{2\pi}{M}\right) z^{-1} + z^{-2}}{1 - 2\rho\cos\left(\frac{2\pi}{M}\right) z^{-1} + \rho^2 z^{-2}} \,, \tag{28}$$

where b_0 and $\rho < 1$ are positive tuning parameters and M is defined by (27). One or multiple notch filters are efficient solutions if the disturbance is located at a single frequency or around a small number of isolated frequencies. If the

disturbance presents non-negligible harmonics at several multiples of a given frequency (i.e. the sensing signal frequency), an effective solution is provided by a comb filter

$$H(z) = \frac{1}{M}\frac{1-z^{-M}}{1-z^{-1}}, \tag{29}$$

which has a very simple structure and allows to eliminate all the frequencies which are integer multiples of f_e. Once the filtered capacitance estimation is obtained, it can be related to the deformation by a look-up table or a polynomial interpolation. In this paper, the second solution is preferred. An advantage of relating capacitance to deformation with a polynomial interpolation rather than using a physical model (see e.g. [24], [27]) is that we can automatically compensate the strain-dependency of the material permittivity, which is typically hard to model. Finally, the overall block diagram of the self-sensing algorithm is shown in Fig. 6.

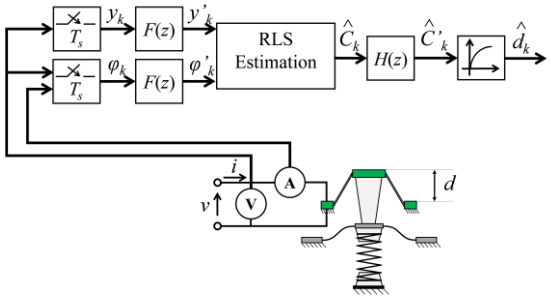

Fig. 6. Self-Sensing algorithm block diagram.

IV. Experimental Results

The proposed self-sensing method is validated by means of the experimental benches shown in Fig. 7 and Fig. 8. The first setup, in Fig. 7, consists of a linear actuator (Aerotech™, Model ANT 25-LA with an Aerotech™ Ensemble ML controller) used to deform the DEA membrane while its displacement is recorded with a Keyence™ LK-G37 laser sensor. A Trek model 610E voltage amplifier is used to send voltage to the DEA. Due to the limited bandwidth of the current sensor embedded in the voltage amplifier, a sensing circuit was designed for measuring the current (range ± 200 μA, accuracy 0.1 %). The second setup is shown in Fig. 8, and is used to test the self-sensing on the overall DEA. The Trek voltage amplifier, the current measurement circuit and the Keyance™ laser displacement sensor are part of this setup as well. A Zaber T-NA08A25 linear actuator and a Zaber T-LA28A linear actuator used to modify the relative position of the two loading springs with respect to the DEA. The algorithm is implemented in LabVIEW with an FPGA data acquisition system working at a sampling frequency of 20 kHz. A first order low-pass pre-filter $F(z)$ with unit gain and time constant τ_f, and a comb filter $H(z)$ tuned according to (29) are also implemented in the overall scheme. The filter time constant τ_f and the RLS forgetting factor μ have been hand tuned in order to achieve minimal peak in the displacement estimation error. Their final values are shown in Table I.

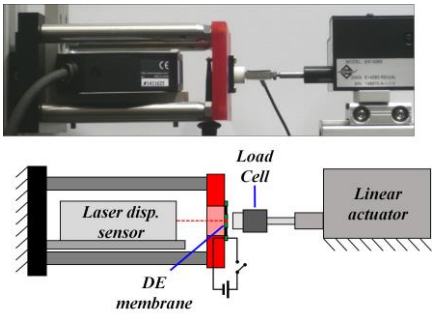

Fig. 7. Experimental setup for testing the DEA membrane, picture (upper) and sketch (lower).

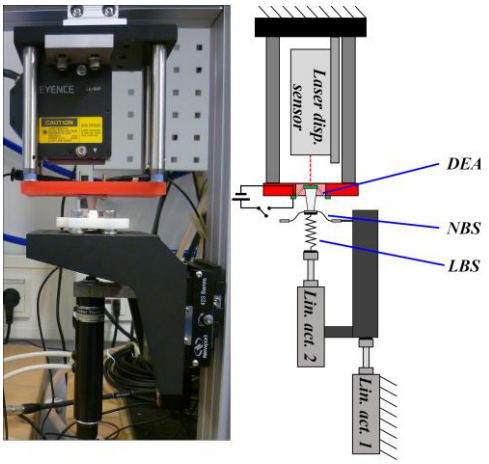

Fig. 8. Experimental setup for testing the DEA system, picture (left) and sketch (right).

TABLE I
SELF-SENSING ALGORITHM PARAMETERS

Parameter	Value	Unit
τ_f	250	[μs]
μ	0.7	[-]

A. Sensing results

In the first set of experiments, the setup shown in Fig. 7 is used to apply a mechanical deformation of 5 mm to the DEA membrane at different mechanical frequencies (0.5, 1 and 2 Hz), while its displacement is recorder with the laser and a high frequency excitation is applied. As suggested in [22], our first choice for the high-frequency sensing signal consists of a sinewave. Several frequencies are tested (200, 400, 600, 800, and 1000 Hz). In this test, the membrane is deformed by an external force and therefore this experiment aims to evaluate the pure sensing capabilities of DEA.

The first step is the evaluation of which of the three model discussed in Section III.A and Section III.B is the most suitable for self-sensing. For this reason, the experimental results corresponding to mechanical frequency of 1 Hz were used as inputs for the self-sensing algorithm based on the three models in (7), (20) and (23). The resulting estimated electrical parameters are plotted in Fig. 9 with respect to the experimentally measured displacement. It can be observed that the best trade-off between accuracy, consistency and computational complexity is provided by the RC series model

in Fig. 5 (b). In fact, the capacitance estimations are consistent at each electrical frequency, and moreover they are in good agreement with the experimental capacitance measurement performed with the LCR-bridge discussed in Section III. The estimation of the series resistance exhibits poor accuracy when performed at lower electrical frequency, but it becomes more consistent as the frequency increases. Moreover, it can be noted how the resistance curves show a hysteretic dependency on the displacement, which is not present in the capacitance. Similar results are obtained by adopting the complete model in Fig. 5 (a), but the resulting leakage resistance estimation is poor. This happens because the value of R_l appears too large in the case under investigation, and its effects are practically unobservable at the selected operating frequencies. Therefore, the complete model for self-sensing seems to introduce an unnecessary increase of computational complexity with respect to the simple RC series model. On the other hand, the purely capacitive model shows poor consistency of the estimated capacitance, which tends to degrade as the sensing frequency changes. If the continuous model is discretized via backward Euler rather than forward Euler (simply replace i_{k-1} with i_k in (23)), the results tend to be more consistent, as shown in Fig. 15. However, there is still a change of the estimated curve depending on the sensing frequency, which is not observed in the RC series model. Therefore, the sensing test suggests that to obtain a self-sensing with a good trade-off between accuracy and computational complexity, the effects of the leakage resistance should be neglected while the electrodes resistance should be included in the model. Fig. 10 shows the capacitance and series resistance estimation obtained at several mechanical frequencies, namely 0.5, 1 and 2 Hz. It can be observed that the capacitance estimations are consistent independently of the electrical or mechanical frequencies, making the capacitance the most suitable parameter for effective self-sensing. The resistance estimations are consistent for a fixed mechanical frequency. Interestingly, the series resistance value tends to increase as the mechanical frequency increases. As the deformation is the same in each test, this result suggests that the series resistance could have some dependency on the material stress. However, this statement requires additional experimental investigation which go beyond the purpose of this paper. Finally, Tables II and III summarize the energetic performance for each test, in terms of average and peak values of the electrical power supplied to the actuator. The power is obtained as the product of measured voltage and current signals. The average power increases for increasing electrical and mechanical frequencies, while the peak power increases for increasing electrical frequency and it is quite insensitive to the mechanical frequency.

B. Self-Sensing results

This section investigates the performance of the algorithm validated in Section IV.B in real-time self-sensing applications. The DEA used as case of study is the same one shown in Fig. 8. The results of the previous section suggest that a better estimation is achieved by using RC series model and higher sensing frequencies, as this allows for a better decoupling between electrical and mechanical behaviors. Moreover, a higher sensing frequency results in a lower order for the comb filter, thus reducing the overall memory requirement. For these reasons, a 100 V, 1000 Hz sensing signal is superimposed to the actuation signal in all the self-sensing experiments. We remark, however, that higher sensing frequencies have the drawback of increasing the power consumption, as highlighted in Tables II and III. The first experiment, shown in Fig. 11, is used for calibrating the capacitance-displacement curve. The calibration is performed with a third order polynomial fitting, which was proven to be sufficiently accurate. The actuation signal consists in a 0.5 Hz unipolar sinewave. Validation is performed with several kind of actuation signals: a filtered, amplitude modulated square wave, a sinesweep from 0 to 2 Hz and a sinesweep from 0 to 10 Hz. The capacitance estimation is used to reconstruct the displacement in real time by means of the previously calibrated polynomial, and the results are shown in Fig. 12-Fig. 14, where the estimated displacement is compared to the measured one. The self-sensing has a remarkable accuracy, since the displacement error is considerably small in each test. The estimation error peak values are always smaller than 1.89 %. The error mean, RMS and peak values are summarized in Table IV.

TABLE II
SENSING RESULTS, AVERAGE POWER CONSUMPTION FOR DIFFERENT ELECTRICAL AND MECHANICAL FREQUENCIES

Average Power [mW]	200 Hz, el.	400 Hz, e.	600 Hz, el.	800 Hz, el	1000 Hz, el.
0.5 Hz, mec.	0.17	0.63	1.33	1.36	1.85
1 Hz, mec.	0.19	0.69	1.42	1.43	1.91
2 Hz, mec.	0.21	0.76	1.54	1.51	1.98

TABLE III
SENSING RESULTS, PEAK POWER CONSUMPTION FOR DIFFERENT ELECTRICAL AND MECHANICAL FREQUENCIES

Average Power [mW]	200 Hz, el.	400 Hz, e.	600 Hz, el.	800 Hz, el	1000 Hz, el.
0.5 Hz, mec.	6.28	13.24	20.02	16.34	18.83
1 Hz, mec.	6.32	13.25	19.95	16.20	18.52
2 Hz, mec.	6.38	13.25	19.67	15.74	17.74

The benefits introduced by the comb filter are illustrated in Fig. 16, where the capacitance signal is shown before (blue) and after (magenta) the filtering process, both in frequency (left) and time domain (right). The capacitance possesses some components at multiples of the estimation frequency (the most relevant appear at 1000, 2000, 4000 and 6000 Hz), and such components are significantly attenuated by the proposed filter.

TABLE IV
SELF-SENSING ERRORS

Experiment	Mean error [%]	RMS error [%]	Peak error [%]
Sinewave at 0.5 Hz	-0.12	1.71	1.74
Sinesweep from 0 to 2 Hz	-0.02	1.17	1.89
Sinesweep from 0 to 10 Hz	-0.18	1.11	1.73
Increasing square wave	-0.66	1.40	1.86

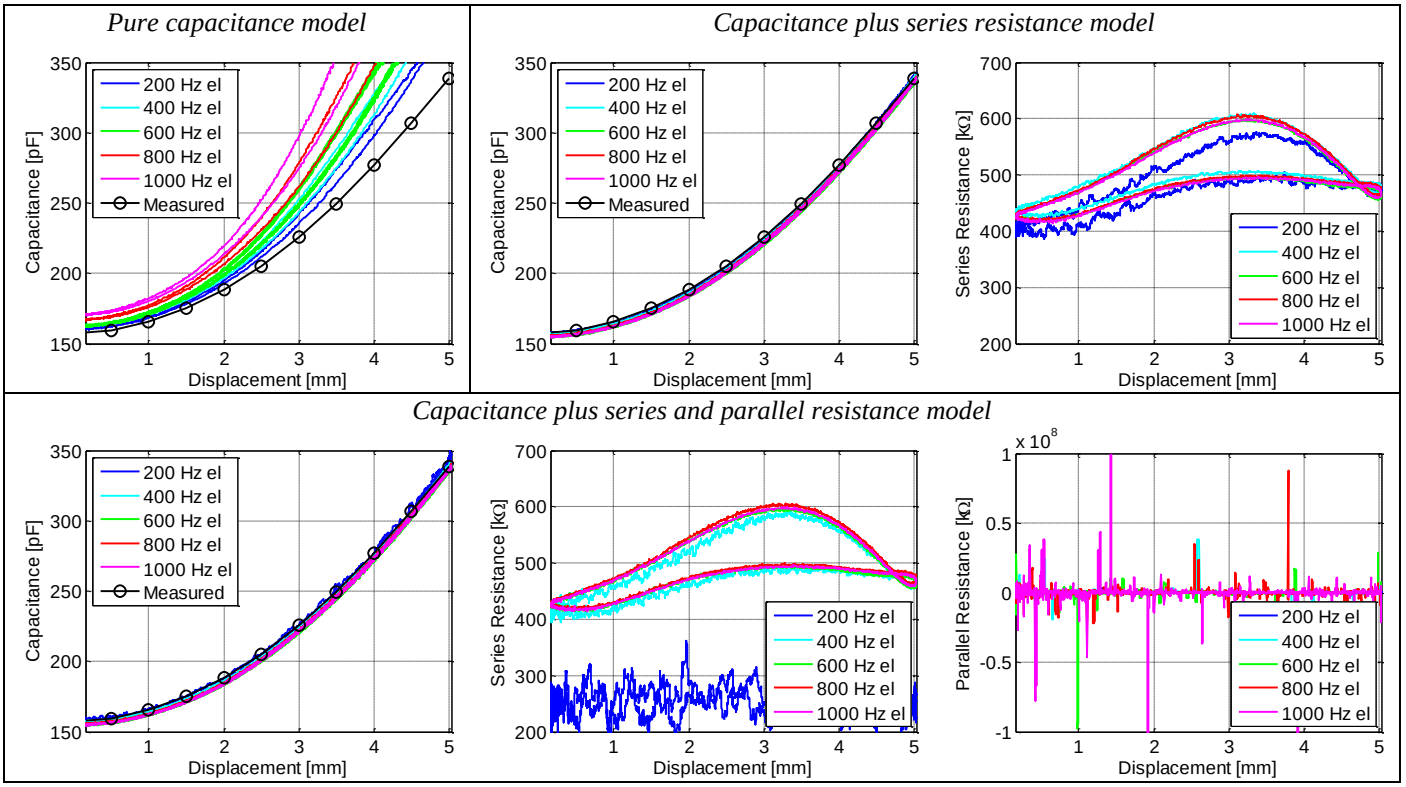

Fig. 9. DEA membrane electrical parameters estimations using 100 V sinusoidal signals at different electrical frequencies (200, 400, 600, 800, 1000 Hz), and deforming the DEA by 5 mm at a mechanical frequency of 1 Hz with an external actuator. Comparison of various electrical models.

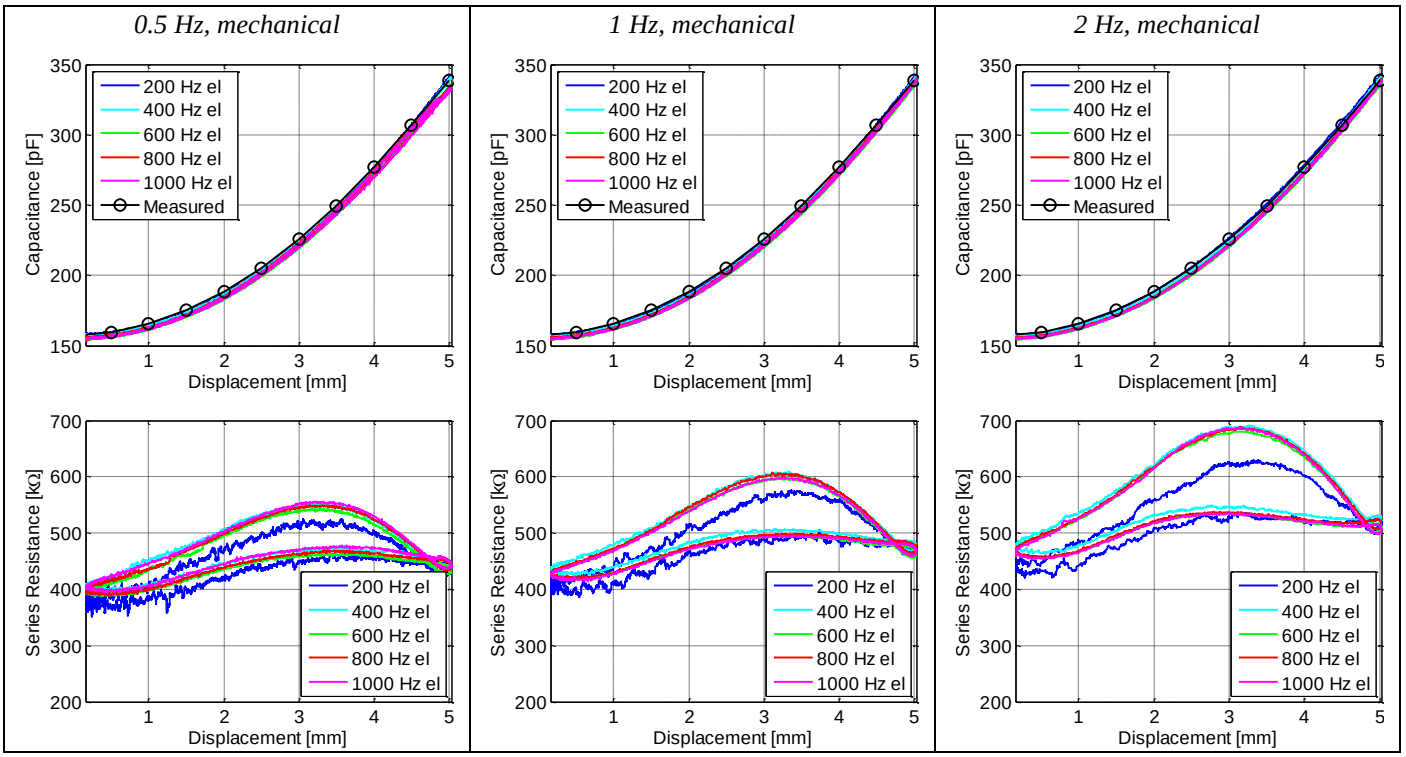

Fig. 10. DEA membrane capacitance and series resistance estimations using 100 V sinusoidal signals at different electrical frequencies (200, 400, 600, 800, 1000 Hz), and deforming the DEA by 5 mm at different mechanical frequencies (0.5, 1, 2 Hz) with an external actuator.

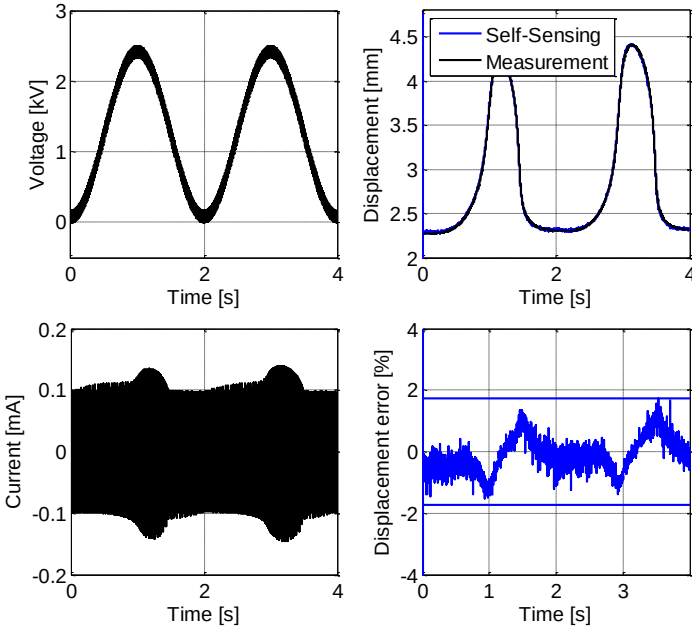

Fig. 11. 0.5 Hz sinewave response voltage, current, displacement and self-sensing error. Peak errors are emphasized with continuous lines.

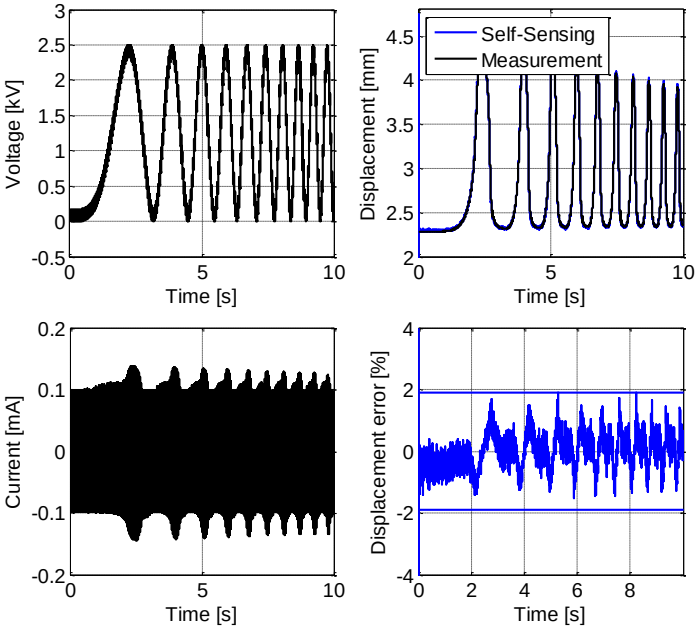

Fig. 13. 0 to 2 Hz sinesweep response voltage, current, displacement and self-sensing error. Peak errors are emphasized with continuous lines.

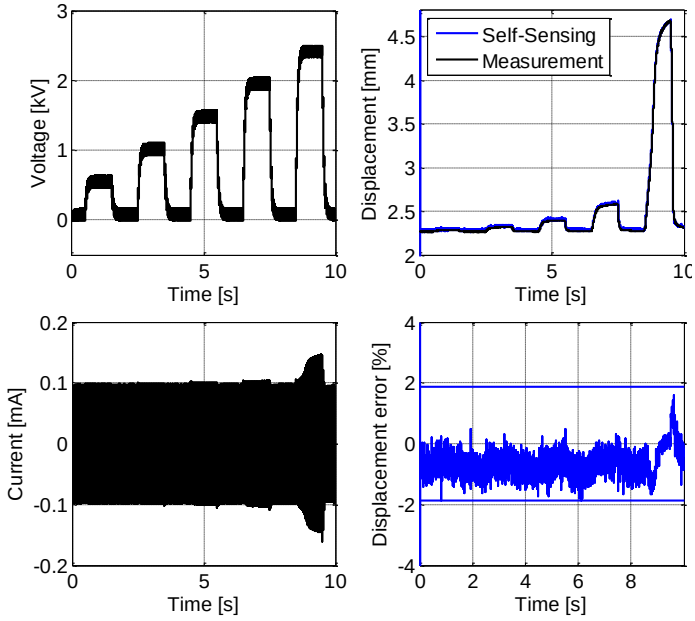

Fig. 12. Increasing amplitude square wave voltage, current, displacement and self-sensing error. Peak errors are emphasized with continuous lines.

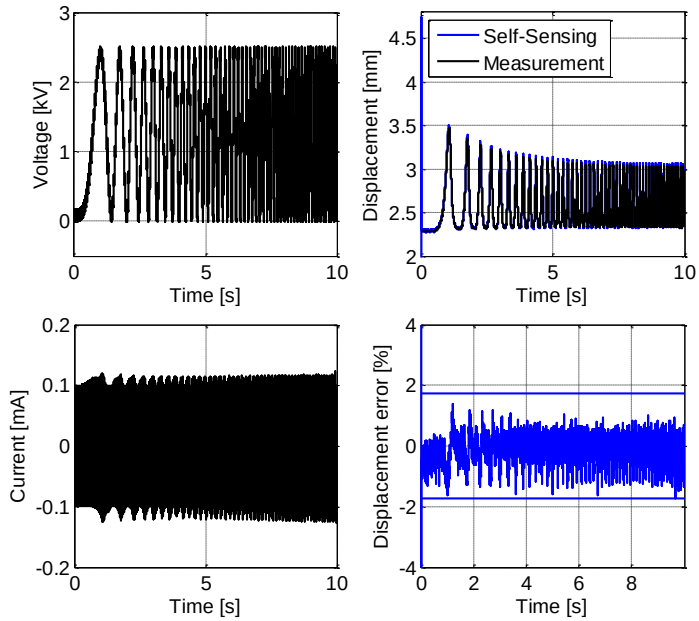

Fig. 14. 0 to 10 Hz sinesweep response voltage, current, displacement and self-sensing error. Peak errors are emphasized with continuous lines.

V. Conclusion

This paper proposed and experimentally validated a self-sensing algorithm for Dielectric Elastomer Actuators. The approach consists of using voltage and current measurements for real-time estimation (via Recursive Least Squares) of the DEA capacitance and electrodes resistance, which can in turn be used to reconstruct information on the deformation of the membrane. The capacitance estimation can be related to the membrane deformation, leading to self-sensing. The validity of the methodology was confirmed by several experiments, proving how the real time estimation algorithm, in conjunction with some ad-hoc filters, enables to reconstruct the actuator deformation with satisfactory accuracy. A comparison between estimated and measured displacement shows that the peak error is always smaller than 1.86 % for a mechanical actuation up to 10 Hz. We also point out that a sufficiently accurate self-sensing was achieved even if the order of persistent excitation of the high-frequency signal, i.e. a sinewave, is not high. This is probably due to the fact that for the simple RC series model, consisting of 2 parameters only, the information provided by a single sinewave having a properly tuned frequency is enough to reconstruct all the system parameters. This may not be true when a 3 parameters model is adopted (including both electrodes and leakage resistance), and more complex sensing signal with a higher order of persisting excitation must be considered to perform a complete identification in such case.

Since the algorithm consists of algebraic operations and difference equations only, it can be successfully implemented in real-time microcontrollers at relatively high rates (20 kHz in this paper). Differently from most of the self-sensing methods presented in literature, the proposed strategy does not require extra measurement or signal processing hardware (e.g. peak detectors, PWM driving electronics, charge sensors, external resistors with voltage sensors), provided that voltage and current measurements are integrated in the driving electronics (which is typically true). Moreover, since the algorithm is based on time-domain rather than frequency domain, different kind of excitation signals can be used without affecting the validity of the result. The combination of online estimation algorithms and digital filtering makes it also possible to perform self-sensing with tunable accuracy and bandwidth. On the other hand, the proposed algorithm requires that the ratio between the sampling frequency and the sensing signal frequency is sufficiently high, in order to let the discretized approximation of the model be admissible. This may represent a limitation in case one is interested in performing self-sensing when having a microcontroller with limited computational capabilities. Therefore, the methodology presented in this work is best suited in case one is interested in a self-sensing solution that can be easily implemented using voltage and current measures directly available in the driving amplifier circuitry, and does not require additional specific sensing or signal processing."

Future developments will be devoted to the analysis of the limits of the proposed approach, the degradation of the capacitance-displacement relationship when operating at different temperatures, the evaluation of alternative self-sensing methods based on charge measurement, the investigation of different kind of high-frequency sensing signals having higher order of persistent excitation than a simple sinewave, and the experimentation of the developed self-sensing methods in closed loop sensor-free control schemes. Moreover, experimental evidence has shown a dependency between the resistance estimation and the membrane force, possibly due to the viscoelastic relaxation process of the electrodes. Therefore, further investigations will be performed to evaluate if also information on force can be extracted from the available signals.

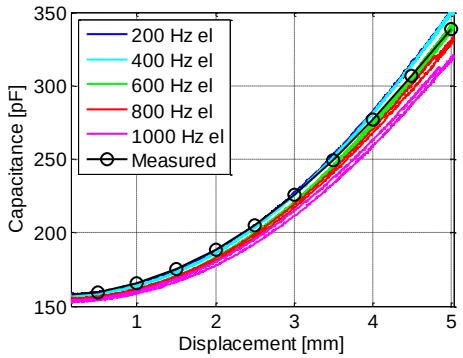

Fig. 15. DEA membrane capacitance estimations, alternative representation of pure capacitance model via backward Euler discretization.

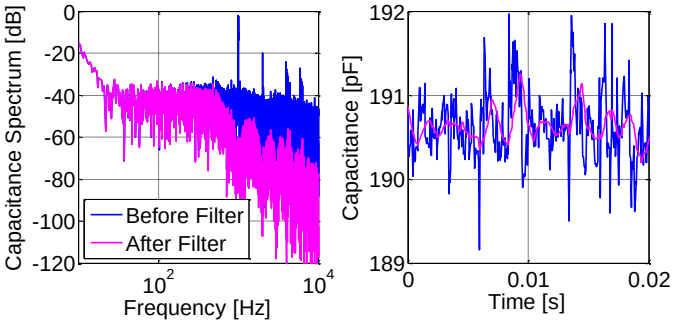

Fig. 16. Estimated capacitance signal, before (blue) and after (magenta) the application of the comb filter, both in frequency (left) and time domain (right).

REFERENCES

[1] F. Carpi, D. De Rossi, R. Kornbluh, R.E. Pelrine, and P. Sommer-Larsen, "*Dielectric Elastomers as Electromechanical Transducers*," Elsevier, Oxford, UK, 2008.

[2] R. Wache, D. N. McCarthy, S. Risse, and G. Kofod, "Rotary Motion Achieved by New Torsional Dielectric Elastomer Actuators Design," *IEEE/ASME Transactions on Mechatronics*, vol. 20, no. 2., pp. 975-977, Apr. 2015.

[3] J. J. Loverich, I. Kanno, and H. Kotera, "Concepts for a new class of all-polymer micropumps," *Lab on a Chip*, vol. 6, no. 9, pp. 1147-1154, Apr. 2006.

[4] M. Giousouf, and G. Kovacs, "Dielectric elastomer actuators used for pneumatic valve technology", *Smart Mater. Struct.*, vol. 22, no. 10, pp. 104010, Sep. 2013.

[5] J. S. Plante, "Dielectric elastomer actuators for binary robotics and mechatronics", Ph.D. dissertation, Dept. of Mechanical Engineering, Massachusetts Institute of Technology, 2006.

[6] G. Jordan, D. N. McCarthy, N. Schlepple, J. Krissler, H. Schroder, and G. Kofod, "Actuated micro-optical submount using a dielectric elastomer actuator", *IEEE/ASME Trans. Mech.*, vol. 16, no. 1, pp. 98-102, Dec. 2010.

[7] C. Lan, C. Lin, and C. Fan, "A Self-Sensing Microgripper Module With Wide Handling Ranges," *IEEE/ASME Transactions on Mechatronics*, vol. 16, no. 1., pp. 141-150, Jan. 2011.

[8] M. Rakotondrabe, I. A. Ivan, S. Khadraoui, P. Lutz, and N. Chaillet, "Simultaneous Displacement / Force Self-Sensing in Piezoelectric Actuators and Applications to Robust Control," *IEEE/ASME Transactions on Mechatronics*, vol. 20, no. 2.. pp. 519-531, Apr. 2015.

[9] G. Rizzello, D. Naso, A. York, and S. Seelecke, "Modeling, Identification, and Control of a Dielectric Electro-Active Polymer Positioning System," *IEEE Trans. Cont. Sys. Techn.*, vol. 23, no. 2, pp. 632-643, Mar. 2015.

[10] M. N. Islam and R. J. Seethaler, "Sensorless Position Control For Piezoelectric Actuators Using A Hybrid Position Observer," *IEEE/ASME Transactions on Mechatronics*, vol. 19, no. 2., pp. 667–675, Apr. 2014.

[11] I. A. Anderson, T. A. Gisby, T. G. McKay, B. M. O'Brien, and E. P. Calius, "Multi-functional dielectric elastomer artificial muscles for soft and smart machines," *Jour. Appl. Phys.*, vol. 112, no. 4, pp. 041101, Jan. 2012.

[12] P. Sommer-Larsen, J. C. Hooker, G. Kofod, K. West, M. Benslimane, and P. Gravesen, "Response of dielectric elastomer actuators," in *SPIE's 8th Annual International Symposium on Smart Structures and Materials*, Aug. 2001, pp. 157-163.

[13] H. Haus, M. Matysek, H. Mößinger, and H. F. Schlaak, "Modelling and characterization of dielectric elastomer stack actuators," *Smart Mater. Struct.*, vol. 22, no. 10, pp. 104009, Oct. 2013.

[14] G. Rizzello, M. Hodgins, D. Naso, A. York, and S. Seelecke, "Dynamic Electromechanical Modeling of a Spring-Biased Dielectric Electro-Active Polymer Actuator System", in *ASME 2014 Conference on Smart Materials, Adaptive Structures and Intelligent Systems*, Sep. 2014, pp. V002T02A012-V002T02A012.

[15] G. Rizzello, M. Hodgins, D. Naso, A. York, and S. Seelecke, "Modeling of the effects of the electrical dynamics on the electromechanical response of a DEA circular actuator with a mass–spring load", *Smart Mater. Struct.*, vol. 24, no. 9, pp. 094003, Aug. 2015.

[16] A. Girard, J.-P. L. Bigue, B. M. OBrien, T. A. Gisby, I. A. Anderson, and J.-S. Plante, “Soft Two-Degree-of-Freedom Dielectric Elastomer Position Sensor Exhibiting Linear Behavior,” *IEEE/ASME Trans. Mechatronics*, vol. 20, no. 1, pp. 105–114, Feb. 2015.

[17] B. O’Brien, J. Thode, I. Anderson, E. Calius, E. Haemmerle, and S. Xie, “Integrated extension sensor based on resistance and voltage measurement for a dielectric elastomer,” in *the 14th International Symposium on: Smart Structures and Materials & Nondestructive Evaluation and Health Monitoring*, Apr. 2007, pp. 652415-652415.

[18] A. York, and S. Seelecke, “Towards Self-Sensing of DEA: Capacitive Sensing Experimental Analysis,” In *ASME 2010 Conference on Smart Materials, Adaptive Structures and Intelligent Systems*, Jan. 2010, pp. 307-314.

[19] Y. Iskandarani, H. R. Karimi, “Sensing Capabilities Based on Dielectric Electro Active Polymers – Feasibility and Potential State-of-the-Art Application,” *IEEE Sensors Journal*, vol. 12, no. 8, pp. 2616-2624, Aug. 2012.

[20] D. Xu, T. G. McKay, S. Michel, and I. A. Anderson, “Enabling large scale capacitive sensing for dielectric elastomers,” In *SPIE Smart Structures and Materials+ Nondestructive Evaluation and Health Monitoring*, Mar. 2014, pp. 90561A-90561A.

[21] N. H. Chuc, D. V. Thuy, J. Park, D. Kim, J. Koo, Y. Lee, J.-D. Nam, and H. R. Choi, “A dielectric elastomer actuator with self-sensing capability,” In *The 15th International Symposium on: Smart Structures and Materials & Nondestructive Evaluation and Health Monitoring*, Mar. 2008, pp. 69270V-69270V.

[22] J. Jung, K. J. Kim, and H. R. Choi, “A self-sensing dielectric elastomer actuator,” *Sensors and Actuators A: Physical*, vol. 143, no.2, pp.343-351, May 2008.

[23] M. Matysek, H. Haus, H. Moessinger, D. Brokken, P. Lotz, and H. F. Schlaak, “Combined driving and sensing circuitry for dielectric elastomer actuators in mobile applications,” in *SPIE Smart Structures and Materials+ Nondestructive Evaluation and Health Monitoring*, Mar. 2011, pp. 797612-797612.

[24] T. A. Gisby, B. M. O’Brien, and I. A. Anderson, “Self sensing feedback for dielectric elastomer actuators,” *Appl. Phys. Lett.*, vol. 102, no. 19, pp. 193703, May 2013.

[25] T. A. Gisby, “Smart Artificial Muscles”, Ph.D. dissertation, Auckland Bioengineering Institute, The University of Auckland, New Zeland, 2011.

[26] S. Rosset, B. M. O’Brien, T. Gisby, D. Xu, H. R. Shea, and I. A-Anderson, “Self-sensing dielectric elastomer actuators in closed-loop operation,” *Smart Mater. Struct.*, vol. 22, no. 10, pp. 104018, Oct. 2013.

[27] T. Hoffstadt, M. Griese, and J. Maas, “Online identification algorithms for integrated dielectric Electro-Active polymer sensors and self-sensing concepts,” *Smart Mater. Struct.*, vol. 23, no. 10, pp. 104007, Sep. 2014.

[28] G. Rizzello, D. Naso, A. York, S. Seelecke, “Self-sensing in dielectric electro-active polymer actuator using linear-in-parametes online estimation,” in *IEEE/IES Int. In Conf. on Mechatronics*, Mar. 2015, pp. 300-306.

[29] M. Hodgins, A.York, and S. Seelecke, “Experimental comparison of bias elements for out-of-plane DEA system,” *Smart Mater. Struct.*, vol. 22, no. 9, p. 094016, Sep. 2013.

[30] L. Riccardi, G. Rizzello, D. Naso, B. Holz, S. Seelecke, H. Janocha, and B. Turchiano, “Modeling and Control of Innovative Smart Materials and Actuators : A Tutorial,” in *IEEE Conference on Control Applications* (*CCA*), Oct. 2014, pp. 965-977.

[31] P. Sommer-Larsen, J. C. Hooker, G. Kofod, K. West, M. Benslimane, and P. Gravesen, “Response of dielectric elastomer actuators”, in *SPIE's 8th Annual International Symposium on Smart Structures and Materials*, Jul. 2001, pp. 157-163.

[32] O. Nelles, “*Nonlinear system identification*,” Springer-Verlag, Berlin, DE, 2001, pp 35-77.

[33] P. C. Wei, J. Han, J. R. Zeidler, and W. H. Ku, “Comparative Tracking Performance of the LMS and RLS Algorithms for Chirped Narrowband Signal Recovery,” *IEEE Transactions on Signal Processing*, vol. 50, no. 7., pp. 1602–1609, Jul. 2002.

[34] N. Bershad, and O. Macchi, “Comparison of RLS and LMS algorithms for tracking a chirped signal,“ in *ICASSP-89.,1989 International Conference on Acoustics, Speech, and Signal Processing*, May 1989, pp. 896-899.

[35] E. Eweda, “Comparison of RLS, LMS, and Sign Algorithms for Tracking Randomly Time-Varying Channels,” *IEEE Transactions on Signal Processing*, vol. 42, no. 11,. pp. 2937-2944, Nov. 1994.

[36] Verhaegen, M. H. "Round-off error propagation in four generally-applicable, recursive, least-squares estimation schemes." *Automatica*, vol. 25, no. 3, pp. 437-444, May 1989.

[37] J. Proakis, “*Digital signal processing: principles algorithms and applications*,” Prentice-Hall of India, Upper Saddle River, New Jersey, U.S., 1996, pp. 343-350.